Integrated 3D Ionic Electrets Electronic Skin (e-Skin) For Harvesting of TENG Energy Through Push-Pull 3D Ionic Electrets and Ion-ion Hopping Mechanism

Ravi Kumar Cheedarala (ravi@chagwon.ac.kr)
Changwon National University
Jung Il Song
Changwon National University

Research Article

Keywords: Sulfonated polyimides (SPI), PEDOT: PSSa, Conducting polymers, TENGS, EMI.BF4 Ionic Liquids, open-circuit voltages (Voc), and short-circuit current (Jsc)

Posted Date: November 29th, 2021

DOI: https://doi.org/10.21203/rs.3.rs-1070606/v1

Abstract

The development of highly durable, stretchable, and steady triboelectric nanogenerators (TENGs) is highly desirable to satisfy the tight requirement of energy demand. Here, we presented a novel integrated polymeric membrane that is designed by PEDOT:PSSa-naphthalene sulfonated polyimide (PPNSP)-EMI. BF_4 **Electronic** skin (e-skin) for potential TENG applications. The proposed TENG e-skin is fabricated by an interconnected architecture with push-pull 3D ionic electrets that can threshold the transfer of charges through an ion-hopping mechanism for the generation of a higher output voltage (Voc) and currents (Jsc) against an electronegative PTFE film. PPNSP was synthesized from the condensation of naphthalene-tetracarboxylic dianhydride, 2, 2'-benzidine sulfonic acid, and 4,4'diaminodiphenyl ether through an addition copolymerization protocol, and PEDOT:PSSa was subsequently deposited using the dip-coating method. Porous networked PPNSP e-skin with continuous ion transport nano-channels is synthesized by introducing simple and strong molecular push-pull 3D interactions via intrinsic ions. In addition, EMI. BF_4 ionic liquid (IL) is doped inside the PPNSP skin to interexchange ions to enhance the potential window for higher output Voc and Iscs. In this article, we investigated the push-pull dynamic interactions between PPNSP-EMI.BF_4 e-skin and PTFE and tolerable output performance. The novel PPNSP- EMI.BF_4 e-skin TENG produced upto 49.1 V and 1.03 μA at 1 Hz, 74 V and 1.45 μA at 2 Hz, 122.3 V and 2.21 μA at 3 Hz and 171 V and 3.6 μA at 4 Hz, and 195 V and 4.43 μA at 5 Hz, respectively. The proposed novel TENG device was shown to be highly flexible, highly durable, commercially viable, and a prospective candidate to produce higher electrical charge outputs at various applied frequencies.

Introduction

For two decades, a drastic increase in global warming, pollution, and carbon emissions has been increasing due to the enormous consumption of fossil fuels and deforestation of plants for energy generation. To overcome the above mentioned challenging issues, clean and renewable energy is an alternative conventional option, such as solar, wind, and tidal energies [1–5]. However, the reduction of the global energy crisis is a major task for scientists and engineers. To accomplish the above demands, unconventional energy harvesting structures are mandatorily required to fill the gap between them, which are mainly piezoelectric, photoelectric, thermoelectric, pyroelectric, electrostatic, and electromagnetic devices. In addition, an additional advantage of these technologies is multifaceted functionality [6]. They can work as portable energy harvesters to drive low-powered electronic devices and work as self-powered sensors to measure various chemical, physical, and biological contributions in an accurate method under various eco-friendly circumstances [7]. In addition, numerous technologies suffer from issues concerning device design limitations, the development of highly efficient composite films, long processing periods, power control circuits, unsteady production performance, packaging, and shelf-life issues. In recent times, triboelectric nanogenerators (TENGs) have established global commitment for the collecting of viable green energy from ambient resources [8]. TENGs were technologically advanced based on a amalgamation of contact separation electrification and electrostatic stimulation for scavenging attenuated mechanical energy via triboelectric resources [9], [10]. The appropriate selection of triboelectric

paired materials and their coherent design can upsurge the rate of energy collection and conversion efficiency [11], [12]. At regular intermissions of TENG resources with oppositely charged electrets, ions or electrons can be driven to movement through the external load and produce a continuous current [13].

In recent times, the use of a sulfonated block copolymer that contains interpenetrating nano-channels and a well-ordered nano-morphology has been proposed to enhance the TENG performance [14]. Inappropriately, these sulfonated block copolymer films are economically not viable due to their complex chemical synthesis and long manufacturing process [15–18]. Therefore, an alternative simple synthetic approach is needed for developing high-performance TENGs using modified sulfonated block copolymers. Sulfonated polyimide block copolymers (SPIs) contain regular porous nanochannels and present numerous manufacturing qualities, such as film forming ability with resilience, elasticity, bendability, stretching ability, long shelf life, and electrochemomechanical properties. SPIs are expected to provide a special physical and chemical morphology, having additional mechanical integrity and limited solvent swelling, owing to the presence of sulfonic acid groups within the ionic network [19]. Although several groups have used a series of SPIs as ionomers for high-performance fuel cell applications and actuators but not applied for TENG applications [20].

A decade ago, Whitesides G. M. et.al. have bring into limelight the ion-transfer system by incorporating ionic clusters into a solid matrix (i.e. styrene polymer, and silica glass,) to produce ionic electrets on the external surface[21–23]. Contact electrification is a process to generate charges through ion transfer by selective transfer of ions that harvests net electrostatic charges. Recently, Watanabe et al. have been developed an SPI for printable polymer actuators integrated from a combination of co-block polyimide, ionic liquid, and carbon materials for high actuation at low input voltage [24]. On the other hand, we have reported a soft actuator based on a 3D ionic network skin made by ultra-fast solution process using sulfonated polyimide block copolymers [20].

Recently, Jang Y. H. have designed conductivity enhancement experiments by mixing of ionic liquids into PEDOT:PSSa conducting polymer for a noteworthy conductivity improvement has been attained by adding ionic liquid (IL)[23]. The ion exchange between PEDOT: PSSa and IL mechanisms can assist PEDOT to decouple from PSSa and harvest bulk-scale conducting domains [25]. Also, they have reported free energy calculations using a density functional system on a simple energy harvesting model using IL pairs and they were loosely bound individuals with the lowest binding energies, which led to the most efficient ion exchange with PEDOT: PSSa conducting polymer [26]. The spontaneous ion exchange followed by nano channeled phase ghettoization between PEDOT and PSSa chains, with formation of a regular π-π stacked PEDOT cations were intercalated by IL anions, is further sustained by molecular dynamics performed on bulk PEDOT:PSSa models in solution[27–31].

PEDOT:PSSa is a combination of polymer mixture of two conductive ionomers. One of the components in this mixture is made up of sodium polystyrene sulfonate and some of the sulfonyl groups are deprotonated and carry a negative charge [32, 33,]. The other component PEDOT is a conjugated polymer that carries positive charges and is based on polythiophene. Together, they exist as charged

macromolecules from a macromolecular sodium salt. PEDOT: PSSa displays the highest efficacy over other conductive organic thermoelectric materials (ZT ~0.42) and thus can be used in flexible and biodegradable thermoelectric generators [34, 35]. The PEDOT chain itself has a PEDOT conjugated polymer with quite a low energy gap and low oxidation potential. For example, world famous AGFA film coats upto 200 million photographic films per year with a thin, extensively stretched layer of virtually translucent and monochrome PEDOT:PSSa as an antistatic mediator to prevent electrostatic discharges through production [36]. Recently, Li et al. developed a strong and highly flexible aramid nanofiber/PEDOT:PSSa film through the vacuum filtration method. A flexible all-solid-state symmetric supercapacitor from an ANF/PEDOT:PSSa film with an operating potential window of 0-1.6 V displays an energy density of 4.54 $Wh.kg^{-1}$ and excellent capacitance retention of 84.5% upto 10000 cycles at room temperature. Extraordinarily, the device was displayed an energy density of 3.83 $W\ h\ kg^{-1}$ with a capacitance retention of 89.5% beyond 5000 cycles, even at -20°C. Moreover, the IL can act as a bridge electrolite between the core SPI polymer and PEDOT:PSSa electrodes, it can provide a further significant intensification of charge distribution performance and extended durability. Recently, Deligoz et al., and Ye et al. were studied the interaction of SPI films with imidazolium cations in various ionic liquids, but they focused on fuel cell applications [37, 38]. From their motivation, we inspired to use a $EMI.BF_4$ ionic liquid for emerging high performance TENG by producing fast ion-hopping rate between cations and hydrophilic $NSP.H^+$, and PEDOT:PSSa conduction layers by ion-ion interactions through porous nano channels. The nano channels can enhance the charge density through the charge transfer complex (CTC), and IL interactions can permit ions to transport easily within the proposed e-skin[39].

To develop an economically viable, highly endurable, and exchange of interionic 3D ionic electrets between electropositive and electronegative membranes when they contact each other, we designed an ionic networked film with continuous and interconnected ion transport nano-channels by using simple and strong atom-level region-specific interactions of hydrophilic and ionic SPI co-blocks with protons (H^+ ions) and anions in the ionic liquid. Additionally, we presented a simple but ultrafast two-step synthesis including dry casting and drop casting for a high-performance TENG. The 3D ionic electrets networked, hydrogen ion(H^+) rich naphthalene sulfonated polyimimide ($NSP.H^+$) ionic membrane, polyethylenedioxythiophene (PEDOT): polystyrenesulfonate (PSSa) as a conducting electrode layer, and 1-ethyl-3-methylimidazolium tetrafluoroborate [EMI. BF_4] ionic liquid (IL) as the mobile electrolyte [20]. Molecular-level region-specific interaction of cations and anions in IL with hydrophilic-hydrophobic co-blocks of NSP mediocre is utilized for building a self-assembled ionic networked polymer with uninterrupted and intersected ion transport nano channels for high-performance TENG [28]. The developed TENG has significant benefits, including hydrophilicity, good solvent exchange, stability in air without further oxidation, high ion exchange capacity, high thermal stability, strong ionic interactions between hydrophilic SPI coblocks and the ionic liquid, ion hopping mechanism, organic PEDOT: PSSa that maintains flexibility and excels a higher TENG voltage and current. Additionally, the IL can act as a strong connection electrolytic solvent between the core NSP ionic membrane and PEDOT: PSSa electrodes through $EMI.BF_4$ can provide a surplus increment of long shelf life without any oxidative degradation[30–31].

Besides, the determination of the present work is to fabricate an ultrafast solvent drop-casting method to produce a combined networked electropositive ionic layer of PEDOT:PSSa-EMI.BF_4-NSP (PPNSP) e-Skin strongly follows an ion-ion hopping mechanism (stages 1 and 2) using 3D ionic electrets. The ionic conductivity and ion exchange capacity of PPNSP are increased up to 3.3 times and 3.5 times through ionic electrets by an ion hopping mechanism that established that the higher density of excess protons (H^+ ions) on the active surface can activate polarized charges to produce a higher TENG output voltage (Voc) and output currents (Isc) when interacting with the electronegative PTFE surface by contact separation mode (stages 3 and 4). The developed PPNSP-PTFE-TENG system is a virtuous candidate for the generation of higher Voc and Isc through a 3D ion-ion hopping mechanism due to its significant benefits, such as a π-π stacked layer that helps to push and pull quick response to travel the ions via interconnected neural networked knots when undergoing contact-separation time. As a result, the novel PPNSP.EMI.BF_4-PTFE TENG produced the Voc and Jsc values from 49.1 V and 1.03 μA at 1 Hz, 74 V and 1.45 μA at 2 Hz, 122.3 V and 2.23 μA at 3 Hz, and 171 V and 3.6 at 4 Hz, and 195.5 V and 4.43 μA at 5 Hz, respectively 92 V and 2 mA, 74 V and 1.4 mA, 52 V and 0.93 mA, 32 V and 0.3 mA open-circuit voltages Voc and Isc at 5 Hz, 4 Hz, 3Hz, 2 Hz, and 1 Hz, respectively, as shown in Figure 1.

Experimental

2.1. Methods

The NSP.H^+, PPNSP and PPNSP-EMI. BF_4 e-skin were determined using FT-IR spectroscopy of IFS66 V/S & HYPERION 3000, Bruker Optiks (Germany),. XRD of the membranes was measured using a DMAX-Ultima III XRD in the class of 5 to 60°. Tensile-Stress Curves and Thermogravimetric Analysis: The tensile strength, modulus properties and elongation of the films have been determined using a table-top universal testing machine (Autograph AGS-5 kN, Shimadzu Corp., Japan.) furnished by a 1 kN load cell with a test speed rate of 10 mm/min. The gauge length among the grips was 10 mm. All samples were cut into a regular rectangular shape. TGA measurements of the composite film membranes were completed on a thermogravimetric analyzer (TG209F3) from NETZSCH (Germany) finished temperatures ranging among 40°C and 800°C in N_2 gas at a heating rate of 10°C/min. All polymeric films were air dried, and SEM interpretations were carried out on an FEI Sirion FE-SEM, 30 kV microscope. The films were carefully dried before capturing the images, and the superficial morphology, and cross-sectional images were studied. The output signals of the all NSP.H^+, PPNSP, PPNSP-EMI.BF_4 e-skin, and PTFE were achieved by intermittently forced and free by income of an oscillator, and the power output was measured using Keithley Digital Multi Meter (KDMM). Consequently, all experiments were determined the impact force via load cell of YC33-5K (SETECH) at numerous frequencies of 1 Hz, to 5 Hz, correspondingly.

2.2. Synthesis of NSP-H+ oligomers

The preparation of an NSP-H^+ co-polyimide membrane with a ≈50% degree of sulfonation (DOS) was conducted. Initially, a 100 mL completely dried 2-neck flask was added to 2.0 g (5.8 mmol) of 4,4'-diamino-[1,1'-bphenyl]-2,2'-disulfonic acid (BDSA)], 20 ml of pure m-cresol, and 3.0 ml (3.6 mmol) of pure

triethyl amine (TEA) successively under nitrogen flow with stirring at room temperature. After BDSA was dissolved, 3.116 g (11.6 mmol) of naphthalene dianhydride (NTDA), 1.16 g (5.8 mmol) of 4, 4'-oxydianiline (ODA), and 1.51 g (2.2 mmol) of phenylformic acid have been added, sequentially. While agitation, the reaction mixture was reached to 80°C and maintained for 4 h, and increased up to 190°C for 20 h and cooled to 70°C. An additional 25 ml of m-cresol was added for diluting the viscous liquid, and then poured into 300 ml of acetone. The polymeric fibers were separated by filtered, cleaned using acetone, and desiccated in vacuum. NSP.H^+.TEA co-polyimide fibers were initially treated with 3 N HCl for 12 h to generate free sulfonic acid (NSP.H^+), washed with DI water, and dried to obtain NSP. H^+ oligomers [20].

2.3. Synthesis of NSP $^-$. H^+ film from NSP$^-$. H^+ oligomers

NSP.H^+ ionic film was prepared by solution casting methods. First, 1.0 g of NSP. H^+ ionic fibers were dissolved in DMSO (15 ml), and stirred for 12 h to obtain a consistent solution, casted on a flat glass Petri dish, and vaporized at 90°C for 24 h to obtain NSP. H^+ film with a thickness of 75 µm[20].

2.4. Fabrication of the PPNSP, and PPNSP-EMI. BF_4 e-Skin from NSP. H^+ film

PPNSP composite film was fabricated by an ultrafast all-solution process. 10 wt% of DMSO was added into the aq. PEDOT:PSSa commercial solution at RT and stirred for 4 h to obtain a PEDOT:PSSa homogeneous solution. Next, the NSP.H^+ film was submerged in a PEDOT:PSSa homogeneous solution for 12 h to generate a precast PPNSP composite membrane, and dried out at 70°C for 5 h. Next, PPNSP e-Skin was immersed in 50% EMI. BF_4 in DMSO for 12 h to generate PPNSP-EMI. BF_4 composite e-skin for the TENG experiments, **Figure. 2**.

2.5. Fabrication of the contact-separation PPNSP-EMI. BF_4 -TENG

The fabrication and working principle of the contact-separation PPNSP e-skin TENGs are discussed. A methodical understanding of PPNSP TENGs has been designated in wide-ranging studies [18, 28]. At this juncture, the assembly of the characteristic model was depicted in **Figure. 6a**. First, NSP.H^+ electrode was cut into sizes of 4 cm × 4 cm = 16 cm^2, and attached on Al electrode layer. Then, the fabricated NSP.H^+-Al conductor was closed to viable flexible foam to decrease the reflecting impact force while contact and separation is progressed. Then, a load cell was linked to the upper part of the Al conductor. A similar protocol was followed for the other two PPNSP-Al and PPNSP-EMI. BF_4 -Al electrodes [40].

Second, the Al electrode was positioned glued on the PTFE film at 4.0 cm × 4.0 cm along with polyurethane flexible foam. In the meantime, a linear oscillator is composed of a DC motor with eccentric arrangement steadily oscillated with a linear slider, as shown in **Figure. 6a**. The maximum oscillation amplitude was 40 mm. The upper portion of the PPNSP-EMI. BF_4 e-skin was adjourned using a cantilever-style beam that was linked to the linear slider. The careful setup of the overall system give rise to in slight

contact between the PPNSP-EMI. BF_4 e-skin, and PTFE film, though the slider oscillation was steady, as shown in **Figure. 6b**[41].

Results And Discussion

3.1. Preparation of Naphthalene SPI (NSP. H^+), NSP. H^+ - PEDOT:PSSa (PPNSP), PPNSP-EMI. BF_4 composite e-skins.

Figure. 2a shows the synthesis of NSP^-. H^+ oligomer film by the sequential addition of monomers of BDSA. TEA, NTDA, and ODA in m-cresol using a literature method by random copolymerization through the addition of copolymers in a one-pot method. Next, NSP.H^+. TEA was subjected to a proton exchange reaction in 3 N HCl to generate NSP^-. H^+ oligomer membrane, **Figure. 2b**. Next, the PPNSP film was fabricated using the solvent dip-coating method by mixing NSP. H^+ oligomer film in 20 wt% PEDOT: PSSa in DMSO, Figure 2c. Later, 3D ionic networked PPNSP-EMI.BF_4 composite film was synthesized using the dip-coating method by immersing the PPNSP film prepared in 20 wt% EMI. BF_4 in DMSO for 12 h, respectively. During dip-coating process, EMI. BF_4 is permeated into the host PPNSP through an ion hopping mechanism through a solvent sorption method. Additionally, long chain oligomers can show inter- and intramolecular charge transfer complex (CTC) singularities intercalated between SO_3H groups with EMI.BF_4. In addition, the hydrophilic SO_3H functional groups were strongly intercalated with each other between PPNSP and EMI.BF_4 through hydrophilic-hydrophilic interactions to generate higher Voc and Jsc (Fig. 1d**)**[40–41].

3.2. Polymerization of PEDOT:PSSa, and Interaction of PPNSP, and EMI.BF_4

Figure 3 shows the mechanistic approach of the formation of PPNSP: EMI. BF_4 e-skin TENG. From oxidation and dimerization of ethylene-dioxythiophene (EDOT) through an oxidative polymerization procedure catalyzed by metal cations, and the universal oxidant is present in various organic solvent systems. Stage-1, showed the oxidation of EDOT(**1**) monomers into unstable cationic radical structures (**2**). The unstable radicals were rearranged into a stable dimer (**3**) by reaction steps that involved combination and deprotonation, as shown in Stage 2. In addition, a neutral PEDOT chain itself has a conjugated network with alternate double bonds with a low energy band gap and low oxidation potential. Ionic interactions were occurred with NSP. H^+, and PEDOT: PSSa to generate the PPNSP e-skin, Stage 3. Next, the PPNSP was soaked in 20% EMI. BF_4 in DMSO to generate the PPNSP: EMI. BF_4 composite e-skin, Stage 4. Continuous recurrence of those steps resulted in the formation of well-dispersed, and doped PEDOT: PSSa solution showed the chemical structures of 3, 4-ethylenedioxythiophene (EDOT), and

poly(3,4-ethylenedioxythiophene) (PEDOT). The structure of the as-prepared PEDOT is made up of benzoid, and quinoid forms. The benzoid structure possesses a π-electron localized, conjugated structure that remains largely unaffected by external sources. In contrast, the quinoid form of PEDOT owns a delocalized state of π-electrons, which can be strongly exaggerated by solvent treatment [42]. In the electrically active, oxidized state, there remains a positive charge on every PEDOT polymer chain. The charges on the backbone were balanced with an anions are from small molecules or a macromolecular anions such as poly(4-styrene sulfonic acid) (PSS). This higher charge transfer performance of the newly developed PPNSP: EMI. BF_4 e-skin TENG through an ion-hopping mechanism that induces high ionic conductivity and tuned the mechanical properties, resulting from strong ionic interactions among the $NSP.H^+$, EMI. BF_4, and PEDOT:PSSa, and interconnected 3D networked polymer matrix[43–46].

3.3. FT-IR, XRD, Stress-strain(SS) curves, and TGA analyses.

FT-IR

FT-IR spectra are quite helpful to identify structural and bonding changes in the synthesized novel NSP-based ionic 3D electret membranes. Figure 4a shows the FT-IR spectra of $NSP.H^+$, PPNSP, and PPNSP-EMI. BF_4 e-skins. The characteristic absorption peaks of $NSP.H^+$ were shown at 628 cm^{-1}(-SO_2), 770 cm^{-1}(-SO_2), 880 cm^{-1}(-SO_2), 1032 cm^{-1}(SNS), 1196 cm^{-1}(v *sym*, O=S=O), 1250 (v, C-N-C), 1344 cm^{-1}(v, CNC), 1453 cm^{-1}(-OH, ben), 1505 cm^{-1} (-CN), 1554 cm^{-1}(v, -C=C), 1674 cm^{-1} (v *asym*, -C=O), 1712 cm^{-1} (v *sym*, -C=O), belong to amide-I, and amide-II, which correspond to the sulfonic acids on the oligomer chains of the NSP polymer. The FT-IR signals of PPNSP showed its typical signatures. For instance, the peaks at 622 cm^{-1}(-SO_2), 695 cm^{-1}(-SO_2), 723 cm^{-1}(SO), 770 cm^{-1}(-SO_2), 830 cm^{-1}(CSC and SO), 921 cm^{-1}(CSC), 1082, cm^{-1}(OCO), 1137 cm^{-1}(C=C), 1193 cm^{-1}(OCO and SO_2), 1451 cm^{-1}(OH, ben), 1498 cm^{-1} (-CN), respectively. The strong stretching bands at 1554 cm^{-1} (v, C=C), 1676 cm^{-1} (v *asym*, -NH-C=O), and 1715 cm^{-1} (v *sym*, -NH-C=O), belonging to amide-I, and amide-II, respectively, were moved to two units due to strong intercalation where ionic-ionic interactions occur between NSP-. H+ and PPNSP membranes. Next, the FT-IR spectrum of the PPNSP-EMI. The BF_4 3D ionic electret membrane is consistent with the chemical structure, which is composed of PPNSP and 1-ethyl-3-methylimidazolium tetrafluoro borate. The EMI. BF_4 shows characteristic bands of C-H stretching in the imidazole ring stretching peaks at 1445 cm^{-1} and 1564 cm^{-1}, imidazole H-C-C, and H-C-N twisting peaks at 925 cm^{-1} and 1191 cm^{-1}, in-plane imidazole ring twisting at 828 cm^{-1}, out-of-plane C-H bending of the imidazole ring at 738 cm^{-1}, and imidazole C-C bending at 598 cm^{-1}, respectively. The stretching peaks appeared at 294 cm^{-1}, 1191 cm^{-1}, 1121 cm^{-1}, 1030 cm^{-1}, 921, cm^{-1}, and 830 cm^{-1}[19]

The strong stretching signals of the BF_4 group appear at 1191 cm^{-1} with a shoulder at 1230 cm^{-1}, and the deformation signals at 738 cm^{-1} and at 658 cm^{-1} strongly support the presence of an imidazolium ring. Additionally, additional strong peaks appearing at 1121 cm^{-1} for SO_2 and 1344 cm^{-1} with a left

shoulder at 1329 cm^{-1} corresponding to the C=N of the imidazolium cation strongly support the presence of EMI. BF_4 in the PPNSP-EMI. BF_4 e-skin. As suggested in Figure 2, ionic clusters are formed by an ultra-ionic exchange reaction between the PPNSP membranes with EMI. BF_4 is well-supported by the FT-IR studies [21].In addition, 3D ionic electrets were developed during slow evaporation of DMSO from hydrophilic PPNSP and EMI. BF_4. Good dispersion of hydrophilic hydrophobic EMI. BF_4 with the core PPNSP polymer enhances interfacial gluing by hydrophilic ionic centers and hydrophilic-hydrophilic ionic interactions and the formation of homogeneous PPNSP.EMI. BF_4 e-skin can display high ionic exchangeability and superior mechanical properties and performs as an ultrafast ion-exchange TENG electrode. The formation of homogeneous and hydrophilic-hydrophilic ionic interactions between NSP. H^+, PPNSP, and PPNSP.EMI.BF_4, through both hydrogen and ionic binding, can display the highest power output through a 3D ionic electret hopping mechanism.

XRD

XRD patterns of the ionic 3D electrets networked $NSP^-.H^+$, PPNSP, and PPNSP-EMI. BF_4 e-skin were depicted in Figure 4b. Broad hallow humps at 18.3 and 23.6 2θ° was found to be amorphous owing to the formation of semi-crystalline components within the polymer network. However, the contains ionic 3D electrets that loosely connect although the ionic bonds between ions and molecules. The XRD pattern of the PPNSP membranes showed a sharp broad peak with superimposition of short crystalline peaks, which indicates strong crystallinity, and the peak appeared at 21.6 θ°. We investigated the XRD pattern of the PPNSP-EMI.BF_4 ionic 3D electret membrane compared with those of the NSP.H^+ and PPNSP membranes. The EMI. BF_4 displayed a plasticizing effect and chelated strongly with both NSP.H^+ and PPNSP to enhance the semi-crystallinity of the membranes. The NSP.H^+ and PPNSP membranes do not show any phase separation due to the formation of strong intercalation through hydrophilicity by ionic-ionic interactions[19, 20] distinct crystalline peaks were at 12.5 and 26.5, 2θ°, showing strong evidence of stretchy crystallinity due to flexible ion-ion interactions within the membrane as a free-flowing network. In addition, the EMI. BF_4 is strongly aggregated on the surface of the PPNSP due to the formation of ionic clusters. The broad peaks that were observed in the NSP.H^+ and PPNSP membranes transformed into sharp peaks at 12.5 and 26.5 2θ°, and the degree of crystallinity is increased due to the establishment of ionic 3D electrets, bridges between NSP.H^+, and PPNSP through EMI.BF_4.

Stress-strain (SS) Curves

With the good deposition of PEDOT:PSSa on top of NSP.H^+ base polymer through strong ionic bonding and reinforcement that can be expected. To demonstrate this reinforcement, tensile tests were performed for 3D ionic electrets, networked PPNSP, and PPNSP-EMI.BF_4 e-skin[20]. Typical stress-strain curves are shown in Figure 4c, and their mechanical properties are compared in Table 1. The NSP. H^+ showed weak behavior and softer behavior and displayed enhanced strain with less strength than PPNSP and PPNSP-EMI. BF_4 membranes. The tensile strength of the NSP. H^+ polymer matrix was showed a lower tensile

strength at 25 MPa, and the strain was 16.6%. The novel PPNSP, and PPNSP.EMI. BF_4 membranes showed enhanced tensile strengths of 32 MPa, and 40.2 MPa and strains were reduced gradually from 10.6 and 8, respectively. The tensile modulus is gradually increased from 1.5 GPa for NSP. H^+, to 3.0 GPa, to 5.0 GPa for PPNSP.EMI. BF_4, respectively. The tensile modulus was increased up to 400% from NSP.H^+ membrane to PPNSP.EMI.BF_4 e-skin by the strong gluing between the membranes through special and interionic interactions between the membranes. Moreover, EMI. BF_4 can penetrate the whole polymeric network through interfacial ionic interactions within NSP and PPNSP to increase the movement of ions between membranes.

Table 1
Stress-strain (SS) curves and elongation at breaks of all the films.

Films	Tensile modulus (GPa)	Tensile Strength (MPa)	Elongation at Break (%)
NSP.H+	1.5	25	16.6
PPNSP	3.0	32	10.6
PPNSP.EMI.BF_4 e-skin	5.0	40.2	8

TGA

Well gluing effect between both PEDOT:PSSa, NSP.H^+, and EMI. BF_4 within the polymer matrix showed superior thermal properties. Figure 4d showed the TGA thermogram of NSP.H^+, PPNSP, and PPNSP-EMI.BF_4 e-skin were differ from each other. They displayed three-stage decomposition; the first stage involved the loss of SO_2 molecules; the second stage involved the decomposition of aromatic polymer chains; and the third stage included the vaporization and elimination of volatile fragments. With the first stage between 50°C and 295°C, almost a 2-6% loss of the initial weight occurs in the case of PPNSP-EMI.BF_4 e-skin, the weight loss is just 1% due to the strong plasticizing effect that occurs with EMI.BF_4 [21]. The second decomposition stage of the NSP.H^+ membrane showed up to 25%, and the other two membranes decomposed up to 60% weight loss at 445°C to 450°C, which involved decay of aromatic ring systems of the polymer. The third stage of decomposition, which ends at approximately 800°C, involves a weight loss of approximately 20% from the carbon chains, which are decomposed into lightweight gases of CO_2, CO, and NH_3 and O_2 gases. The thermogram of the NSP. H^+ membrane differs from that of PPNSP and PPNSP-EMI.BF_4 e-skin. This change might render due to PPNSP, and PPNSP-EMI.BF_4 e-skin were hydrophilic after EMI doping. BF_4, and destroyed the crystalline structures. Eventually, after mixing with EMI.BF_4, the structure of the PPNSP becomes irregular, with deterioration of the thermal properties.

3.3 SEM analysis of NSP.H^+ , PPNSP, and PPNSP-EMI. BF_4 composite films

Scanning Electron Microscopy (SEM) images of the NSP.H^+ and PPNSP films are shown in Figure 5 and reveal the surface morphologies. In particular, Figures 5a, and 5b show the wrinkle-free plain surface with no obvious changes. However, the inbuilt hydrophilic -SO_3H groups were attached to the host polyimide co-blocks that could intercalate and generate nano level distances between the oligomeric networked chains. Significant submicron-sized porous grooves and micron-sized crests with tightly packed networks were found on the surface, as shown in **Figure. 5c**. The hollow groves and crests were created due to a significant 3D ionic network on the surface morphology. In the cross-sectional view, hydrophilic and hydrophilic interactions take place between NSP.H^+, and PEDOT:PSSa through hydrogen bonding that created a loosely bound network between them, Figure 5d [21]. The hydrophilic-hydrophilic ionic system can establish a flexible interpenetration complex between NSP^--H^+ and PEDOT:PSSa to improve the charge densities on the polymeric surface. The 3D ionic networked morphology can exchange ions through strong ionic knots, which can travel through hydrophilic ionic channels and strongly support the ion hopping mechanism. After impregnation of EMI.BF_4 IL, the thickness of PPNSP e-Skin was increased due to swelling of ionic liquid. Figure 5e shows the strong spherical aggregations on the surface by 3D ionic clusters. In addition, the inset image clearly indicates the 3D ionic clusters at nanoscale levels. In the cross-sectional view, a loosely bounded net-like channeled network appears due to the strong intercalation between PEPDOT:PSSa and EMI.BF_4 IL. Additionally, the high-resolution surface and cross-sectional images display the formation of zigzag net-like channels. In particular, EMI^+ cations were deposited on the hydrophilic regions as bright spots, which clearly indicate the formation of PPNSP-EMI^+ by an ion hopping mechanism, as shown in Figure 5f. The homogeneity of the blend membrane confirmed the strong ionic interactions, which included ionic cross-linking and hydrogen bonding between EMI.BF_4 and the PPNSP composite membrane, resulting in the enhanced interfacial compatibility and mechanical stiffness of the composite membrane. In addition, ionic cross-linking and hydrogen bonding can generate higher charges on the surface. These charges can enhance the open circuit voltage and short circuit currents. The overall morphologies were strongly justified to accelerate the charges within the charge transfer complexes when a contact-separation mode TENG was performed [25, 39].

Set-up Of Ppnsp-emi. Bf4 E-skin Teng For Generation Of Voltages And Currents

Figures 6a-b shows the mechanical setup of the PPNSP-EMI.BF_4 e-skin TENG in full separation and contact mode of state, periodically, to generate the actual triboelectric current. The energy harvesting principle strictly follows the contact electrification approach by the contact and separation of PPNSP-EMI. BF_4 and PTFE under various applied frequencies. The working principle of the proposed PPNSP-EMI. The BF_4 e-skin TENG was explained by the PPNSP surface, and the aluminum (Al) electrodes were

initially free of charges (Figure 6c). When the oscillation was underway by the linear slider by the DC motor, the triboelectrically negative PTFE was in superficial contact on the surface of PPNSP-EMI.BF_4. The PTFE surface was converted to temporarily negatively charged and, in contrast, PPNSP-EMI.BF_4 turned positive owing to the contact electrification process (Figure 6d). During the contact electrification process, the generated electrical charges are retained on the surface for a longer time due to the insulating properties of the surface. The PTFE surface showed superior charge separation when it was separated from PPNSP-EMI.BF_4 e-skin. At this time, the Al electrodes were strongly persuaded to collect charges by PPNSP-EMI. The BF_4 e-Skin and PTFE surfaces remained neutral, the top electrode was positively charged, and the bottom electrode was negatively charged. During the separation process, the generated charges were transformed through an external load, and current flow occurred (Figure 6e). When the two electrodes were completely separated, the current was clogged and reached the equilibrium state (Figure 6f). When both the surfaces of PPNSP-EMI.BF_4 e-Skin and PTFE were locked together, and the electrostatic induction was high and broke the equilibrium state, resulting in charge redistribution of Al electrodes via acceptance and release of ions, as shown in Figure 6g. As a result, the current flows in the reverse direction. Till the two polymeric layers were fully contacted, the charge-transfer process disappeared, and no charges were generated at all [41].

4.1. TENG result of NSP. H^+-PTFE, PPNSP-PTFE, and PPNSP-EMI. BF_4 e-skin-PTFE

To authenticate the TENG principle, we first investigated the electric output of the NSP.H^+ against the PTFE film through the contact separation mode. The open-circuit Voc of the NSP.H^+ at 1 Hz surged from −11.6 V to 13.6 V upon separated. Additionally, the charge transferred between the Al electrodes instantaneously generated a short-circuit current Jsc. The peak value of Jsc reached from −0.057 μA to 0.062 μA, as shown in Figures 7a-b. By gradually changing the speed of the linear motor from 1 Hz to 5 Hz, different Voc and Jsc values were observed. The generated Voc and Jsc were achieved from −20.6 V to +23.1 V, −0.0.26 μA to 0.26 μA at 2 Hz, from −28.5 V to 32.6 V and from −0.27 μA to 0.35 μA at 3 Hz, and from −35.5 V to 41 V and from −3.7 μA to 0.43 μA at 4 Hz and -45.2 to 51.7 V and -0.62 μA to 0.72 μA at 5 Hz, respectively. Next, the Voc and Jsc of the PPNSP TENG showed an output voltage of -19.2 V to 21.5 V and from −0.32 to 0.36 μA at 1 Hz, from −33 V to 38 V and from −0.44 to 0.49 μA at 4 Hz, from −52 V to 59 V, and from −0.81 to 0.9 μA at 3 Hz, from −63.3 to 73 V, and from −1.1 to 1.37 μA at 6 Hz, -76.5 V to 88 V and -1.44 μA to 1.6 μA, respectively, as shown in Figures 7c-d. Significant enhancements were observed in both voltage and current after doping with EMI. BF4 IL into the PPNSP film by dip-coating method. Significant enhancement was observed in both voltage and current after doping with EMI. BF_4 IL into the PPNSP film by dip coating method. The homogeneous deposition EMI.BF_4 into PPNSP, quantum jump enhancement was observed, and the quantitative output performance of PPNSP-EMI was determined. BF_4 due to active mobility of EMI. BF_4 ions within the host PPNSP polymer film as well as the surface. The PPNSP-EMI. BF_4 –PTFE TENG provided Voc and Jsc values from −22.9 V to 26.2

V and from −0.48 μA to 0.55 μA at 1 Hz, from −34 V to 40 V and from −0.68 μA to 0.77 μA at 2 Hz, from −57.1 V to 65.2 V and from −1.02 to 1.21.08 μA at 3 Hz and from −80 V to 91 V and from −1.68 to 1.92 μA at 4 Hz and -86.5 V to 109 V and -2.08 to 2.35 μA at 5 Hz, respectively, as shown in Figures 7e-f. In specific, it can be seen that the PPNSP-EMI. The BF_4-PTFE TENG showed higher electrical output than the other two systems (i.e., NSP.H^+-PTFE, and PPNSP-PTFE TENG) owing to the availability of abundant mobile BF_4^- ions from EMI.BF_4 IL. The present result have been justified the concept of by the Jang. Y. H. et al and displayed higher conductivity through our PPNSP-EMI.BF_4 e-skin TENG in comparison with NSP.H^+ and PPNSP TENGs due to the addition of EMI.BF_4[24].

4.2. Performance Characteristics of PPNSP.EMI. BF_4-PTFE TENG

Additional experiments of load resistance analysis, power densities, and device constancy, were carried out using the PPNSP.EMI.BF_4 e-skin-PTFE TENG at 5 Hz applied frequency, as shown in Figure 8. The peak instantaneous Voc and Isc of PPNSP.EMI.BF_4 e-skin-PTFE TENG were measured at 5 Hz oscillation. It was noted that the peak Voc decreased with increasing resistance, whereas Jsc increased. Consequently, the device output increased when the load resistance was increased from 100 ohm Ω to 570 MΩ. The areal power density of the proposed device at a 5 Hz applied load was evaluated using the following equation.

$P_A=V^2/(R\cdot A)$

Where V is the generated output voltage from PPNSP.EMI.BF_4-PTFE TENG device, R is the load resistance, and A is the device area (A= 4cm x 4 cm=8 cm^2). The areal power density of the device was 33.2 mW, and the load resistance was 570 MΩ. This indicated that 570 MΩ was the load-matching resistance for achieving the maximum output power required for real-time applications, as shown in Figure 8a. The unidirectional output can be stored in energy storage systems such as capacitors, and batteries and the rectified Voc of PPNSP.EMI.BF_4-PTFE TENG device is shown in Figures 8b, and 8c. The performance stability of Voc and Jsc of PPNSP.EMI. BF_4-PTFE TENG system was checked at a 5 Hz applied frequency, and it was stable for ~10000 cycles without any fluctuations (Figures 8d, and 8e). The durability and stability of the proposed system showed exceptional harvesting properties and superior mechanical strength.

The performance of Voc and Jsc of NSP.H^+-PTFE-TENG>PPNSP-PTFE-TENG >PPNSP-EMI.BF_4 e-skin-PTFE-TENGs. The e-skin-TENG gradually increased with increasing ionic density both inside the network and outside the surface. Next, when the impact force was increased by the oscilloscope, surface charges were generated through the 3D ion hopping induction mechanism and surged the higher Voc and Jsc values. The output Voc, and Jsc of PPNSP.EMI.BF_4-TENGs produced 316% and 300% at 5 Hz, respectively, as shown in Figures 9a, and 9b. The load cell YC33-5K (SETECH) was utilized to measure the

contact force, and the results are shown in Figure 9c. Based on the obtained research data, the impact force was gradually increased with respect to the applied contact frequencies. When the impact force is high, an additional effective area is induced, and subsequently, higher output voltage and currents are generated. The Voc values of PPNSP.EMI. BF_4-TENGs are 1.6 and 2.6 times higher than that of PPNSP-PTFE-TENG and NSP-PTFE-TENG at 5 Hz, and the Jsc values of PPNSP.EMI.BF_4-TENGs are 1.8 and 4 times higher than that of PPNSP-PTFE-TENG and NSP-PTFE-TENG at 5 Hz, respectively, due to strong 3D ionic interactions occurring through an ion hopping mechanism to transport ions. Additionally, a mechanistic explanation is suggested when EMI occurs. BF_4 IL interacts with the ionic sites of NSP and PPSNP polymers and exchanges ions. The Voc and Isc of PPNSP.EMI.BF_4-TENGs showed superior triboelectric properties compared to PPNSP-PTFE TENGs and NSP TENGs owing to the availability of large ionic clusters by invasion of EMI. BF_4 IL within the 3D networked channels inside and on the surface of the polymer network. Therefore, we modified the NSP, PPSNP, and PPNSP.EMI.BF_4 composite surfaces for generating high power output through doping of EMI. BF_4 into the NSP. H^+, and subsequently, dip coating of the PEDOT:PSSa conducting polymer to generate higher ionic conductivities. Next, we conducted experiments to regulate the impact force at various applied frequencies.

Conclusion

In this research, we have demonstrated a 3D ionic networked polymer TENG based on PPNSP.EMI.BF_4-PTFE with ion-ion hopping alternates hydrophilic nano-channels integrated with sulfonic acid groups, resulting in superior electro-chemo-mechanical properties. Well-arranged hydrophilic sulfonic acid groups have good compatibility with both PEDOT:PSSa, and EMI. BF_4 to penetrate at atom-atom interactions owing to PPNSP.EMI. The BF_4 composite film thereby provided constant interconnected ion-ion interactions to transport charges through ionic nano-channels to enhance Voc and Jsc performance and robustness. The FE-SEM analysis clearly revealed the ion-ion nano-channels within the polymer network that trigger the charges very fast when PPNSP.EMI. BF_4 e-skin interacted with the PTFE surface. The SS curves of the NSP.H^+, PPNSP, and PPNSP.EMI. BF_4 noticed the strong flexibility and resilience of the membranes to be compatible with the contact-separation mode TENG without damaging the membranes even after several cycles of contact-separation mode TENGs. Mainly, the PPNSP.EMI. BF_4 e-skin displayed a dramatic increase in the tensile modulus, up to 131%, tensile strength, up to 174%, and elongation at break values up to 277% compared to those of its starting membranes, such as the NSP.H^+ and PPNSP membranes. These synergistic effects were beneficial after incorporation of EMI. BF_4 IL in the PPNSP membrane in designing a high-performance ion-mediated e-skin-based TENG that shows large affective charge induction to provide higher Voc and Jsc. In particular, the NSP-H^+ membrane was sandwiched by the PEDOT:PSSa conducting polymer, which enhanced superior conductivities.

The Voc and Jsc of the NSP. H^+ at 5 Hz surged upto -45.2 to 51.7 V and -0.62 µA to 0.72 µA, respectively. Next, the PPNSP TENG showed an output voltage of at 5 Hz, -76.5 V to 88 V and -1.44 µA to 1.6 µA, respectively. On the other hand, PPNSP-EMI. BF_4 e-skin was shown upto -86.5 V to 109 V and -2.08 to

2.35 μA at 5 Hz owing to EMI. The BF_4 IL interpenetrated within the polymer network, which enhanced the accumulation of high power densities. Significant enhancement was observed in both voltage and current after doping with EMI. BF_4 IL into the PPNSP film by dip coating method. The homogeneous deposition EMI. BF_4 into PPNSP, quantum jump enhancement was observed, and the quantitative output performance of PPNSP-EMI was determined. BF_4 due to active mobility of EMI. BF_4 ions within the host PPNSP polymer film as well as the surface. In specific, it can be seen that the PPNSP-EMI. The BF_4-PTFE TENG showed higher electrical output than the other two systems (i.e., NSP. H^+-PTFE, and PPNSP-PTFE TENG) owing to the availability of abundant mobile BF_4^- ions from EMI. BF_4 IL. Next, Performance Characteristics of PPNSP.EMI.BF_4-PTFE TENG showed the load resistance analysis, power density calculations, and device stability at 5 Hz applied frequency, and load resistance was increased from 100 ohm Ω to 570 MΩ. The areal power density of the device was 33.2 mW, and the load resistance was 570 MΩ. Additionally, the unidirectional output was stored in energy storage systems such as capacitors and batteries and the rectified Voc of PPNSP.EMI.BF_4-PTFE e-skin TENG device. The performance stability of Voc and Jsc of PPNSP.EMI. The BF_4-PTFE TENG system was checked at a 5 Hz applied frequency, and it was stable for ~10000 cycles without any fluctuations. The durability and stability of the proposed system showed excellent harvesting performance and superior mechanical strength without any surface damage. The present results have suggested that the controlled self-assembly process for strong ion-ion connections and ion transport nanochannels can be used for tailoring superior TENG applications, which are potentially required for next-generation electronic products such as wearable soft electronics, flexible displays, and smart mobile phones.

Declarations

Acknowledgements

This work was supported by the National Research Foundation of Korea (NRF) grant funded by the Korea government (MSIP) No. 2017R1A2B2011730, No. 2018R1A6A1A03024509 and 2019R1A2C1011113.

Declaration of Interest Statement

We believe that this article will clearly suggest broad interest in both academic and industrial fields, because we develop simple but novel fabrication process for “**Integrated 3D Ionic Electrets Electronic Skin (e-Skin) for Harvesting of TENG Energy through Push-Pull 3D Ionic Electrets and Ion-ion Hopping Mechanism”**

We believe that our work represents a timely methodological and scientific advance – even a breakthrough - in the field of both materials science and mechanical engineering, and thus is appropriate for a journal with the scope and readership of **Nano Energy**, we are excited to share our manuscript with you and look forward to your response.

We also declare that this work has not been submitted with any scientific journal.

Regards,

Ravi Kumar Cheedarala.

References

1. Qin, Y., Wang, X. & Wang, Z. L.Nature, 451(2008)809–813
2. Xu, S. *et al.*Nature nanotechnology, 5(2010)366–373
3. Fan, F. R., Zhu, L. L. G., Zhang, W. W. R. & Wang, Z. L.Nano letters, 12(2012)3109–3114
4. Wang, Z. L., Chen, J. & Lin, L.Energy & Environmental Science, 8(2015)2250–2282
5. Fan, F. R., Tian, Z. Q. & Wang, Z. L.Nano Energy, 1(2012)328–334
6. Fan, F. R. *et al.*Nano Lett. 12(2012)3109–3114
7. Zhu, G. *et al.*Nano Lett., 12(2012)4960–4965
8. Wang, S., Lin, L. & Wang, Z. L.Nano Lett., 12(2012)6339–6346
9. Zhu, G. *et al.*Nano Lett., 13(2013)847–853
10. Niu, S. *et al.*Energy & Environmental Science, 6(2013)3576–3583
11. Zhao, D., Duan, L. T., Xue, M. Q., Ni, W. & Cao, T. B.Angew. Chem. Int. Ed., 48(2009)6699–6703
12. Bandodkar, A. J., Jeerapan, I. & Wang, J.ACS Sensors, 1(2016),464–482
13. Lowell, J. & Rose-Innes, A. C.Adv. Phys., 29(1980)9947–1023
14. Imaizumi, S., Kokubo, H. & Watanabe, M.Macromolecules, 45(2013),401
15. Gao, R., Wang, D., Heflin, J. R. & Long, T. E.J. Mater. Chem., 22(2012),13473
16. Vargantwar, P. H., Roskov, K. E., Ghosh, T. K. & Spontak, R. J.Macromol. Rapid Commun., 33(2012),61
17. Wang, X. L., Oh, I. K., Lu, J., Ju, J. & Lee, S.Mater. Lett., 61(2007),5117
18. Wang, Z. L. & Nano, A. C. S. 7(2013)9533–9557
19. Cheedarala, R. K., Duy, L. C. & Ahn, K. K.Nano Energy, 44(2018)430–437
20. Cheedarala, R. K., Jeon, J. H., Kee, C. D. & Oh, I. K.Adv. Funct. Meter., 24 (2014)6005–6015
21. Soh, S., Kwok, S. W., Liu, H. & Whitesides, G. M.J. Am. Chem. Soc., 134(2012)20151–20159
22. McCarty, L. S., Winkleman, A. & Whitesides, G. M.J. Am. Chem. Soc., 129(2007)4075–4088
23. Izarra, A. D., Park, S., Lee, J., Lansac, Y. & Jang, Y. H.J. Am. Chem. Soc., 140 (2018),5375–5384
24. Lee, S. Y. *et al.*J. Am. Chem. Soc.132(2010),9764
25. Inganas, O.Nat. Photonics, 5(2011)201
26. Na, S. I., Kim, S. S., Jo, J. & Kim, D. Y.Adv. Mater., 20, (2008)4061
27. Pei, Q., Zuccarello, G., Ahlskog, M. & Inganas, O.Polymer, 35(1994),1347
28. Groenendaal, L. B., Jonas, F., Freitag, D., Pielartzik, H. & Reynolds, J. R.Adv. Mater., 12(2000)481
29. Elschner, A., Kirchmeyer, S., Lovenich, W., Merker, U. & Reuter, K. *PEDOT: Principles and Applications of an Intrinsically Conductive Polymer* (CRC Press, Boca Raton, FL, 2010).

30. Crispin, X. *et al.*Chem. Mater., 18(2006)4354
31. Kim, Y. H. *et al.*Adv. Funct. Mater., 21(2011)1076
32. Vosgueritchian, M., Lipomi, D. J. & Bao, Z.Adv. Funct. Mater., 22(2012)421
33. Pinto, N. J. *et al.*Sensors and Actuators B: Chemical, 156(2011)849–853
34. Tintula, K. K., Pitchumani, S., Sridhar, P. & Shukla, A. K.Bulletin of Materials Science, 33(2010)157–163
35. He, X. *et al.*J. Liu, Materials, 10 (2017)220
36. Li, Y. *et al.*J. Meter. Chem. A, 4(2016)17324–17332
37. Deligoez, H. & Yilmazoglu, M.J. Power Sources, 196(2011)3496
38. Ye, Y. S. *et al.*J. Mater. Chem.21(2013)10448
39. Jeon, J. H., Cheedarala, R. K., Kee, C. D. & Oh, I. K.Adv. Funct. Meter., 23 (2013)6007–6018
40. Shi, W., Zhao, T., Xi, J., Wang, D. & Shuai, Z.J. Am. Chem. Soc., 137(2015)12929
41. Cheedarala, R. K., Parvez, A. N. & Ahn, K. K.Nano Energy, 53(2018),362–372
42. Cheedarala, R. K., Shahriar, M., Ahn, J. H., Hwang, J. Y. & Ahn, K. K.Nano Energy, 65(2019),104017
43. McCarthy, J. E., Hanley, C. A., Brennan, L. J., Lambertinib, V. G. & Gun'ko, Y. K.J. *Mater. Chem. C*, 2(2014)764–770
44. Kim, S., Kim, H. S. & Park, Y. D.Organic Electronics, 30(2016)296–301
45. Cheedarala, R. K. & Song, J. I.Frontiers in Nanotechnology, 3(2021)30
46. Cheedarala, R. K. & Song, J. I.International Journal of Smart and Nano Materials, 11(2020)38–46
47. Cheedarala, R. K. *3D Ionic Networked Hydrophilic-Hydrophobic Nano Channeled Triboelectric Nanogenerators,(Book Chapter), Novel Nanomaterials (book)* (Intech Open, Publishers., London, UK, 2021).

Figures

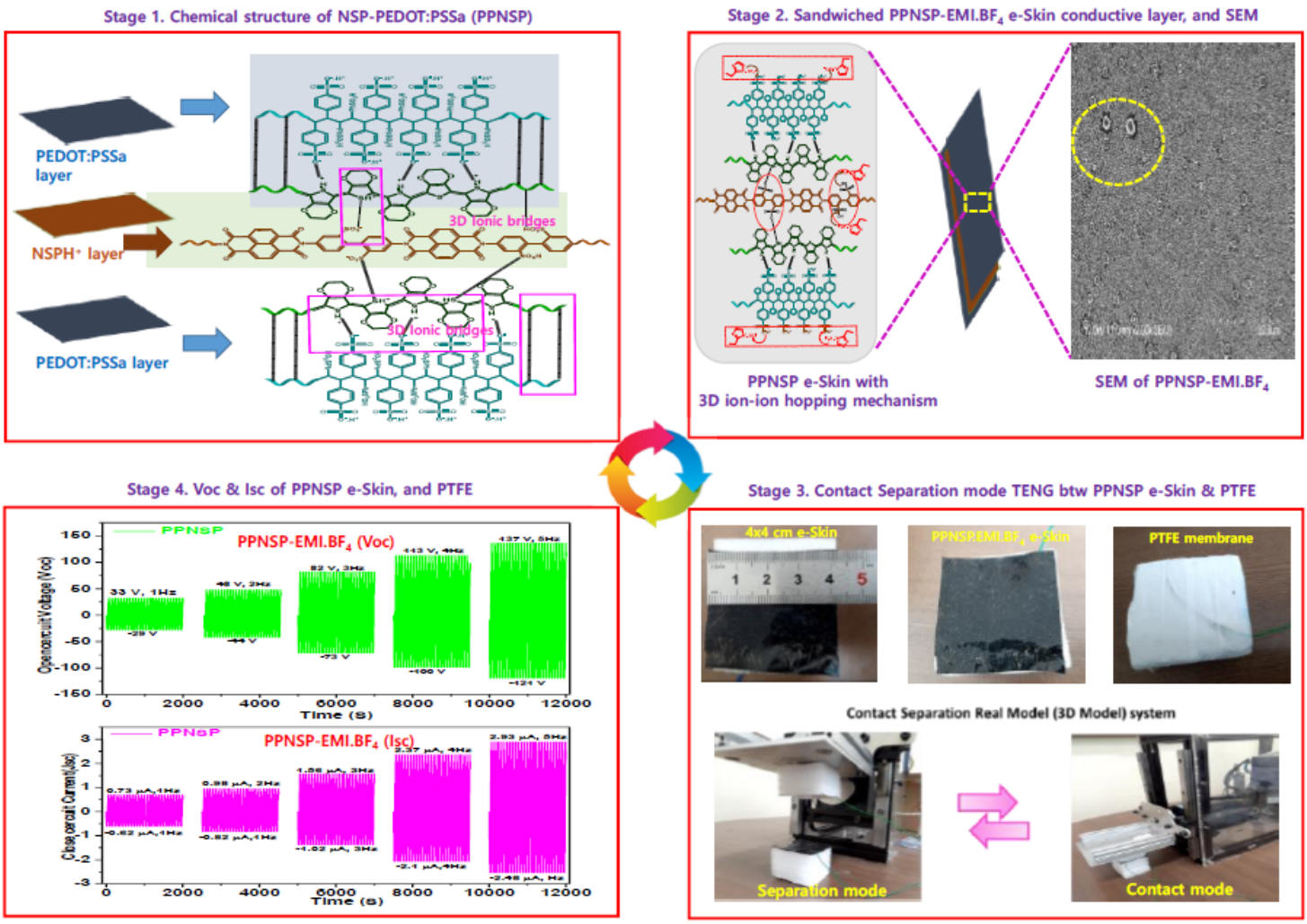

Figure 1

Schematic representation of PPNSP-EMI.BF4-PTFE TENG for harvesting energy through 3D ionic electrets and ion-hopping mechanisms. Stage 1. Synthesis of NSP.H+s: PEDOT:PSSa composite film, Stage 2 Fabrication of 3D ionic net-worked conductive composite electronic skin (e-Skin); Stage 3. Size of (4 cmx 4 cm) PPNSP.EMI.BF4 e-skin and PTFE, and vertical contact separation mode TENG; Stage 4. The Voc and Jsc of conductive PPNSP-EMI. BF4-PTFE e-Skin TENG.

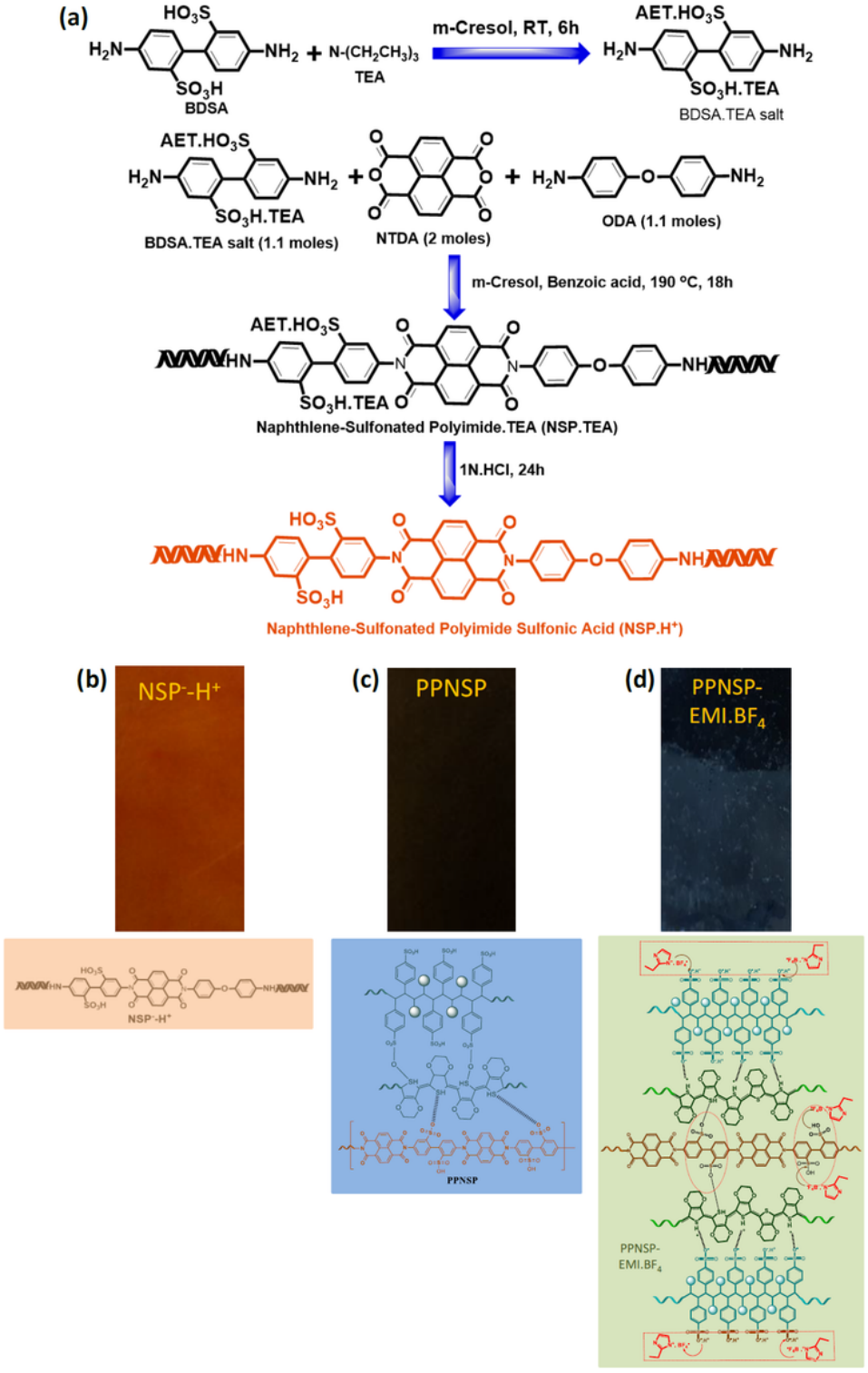

Figure 2

a) Synthesis method of NSP. H+, and digital images and chemical structures of b) NSP.H+, c) conjugated conductive PEDOT:PSSa film; d) ion hopping mechanism between PPNSP and EMI. BF4 with strong ionic-ionic interactions between host PPNSP and guest EMI. BF4 for generation of higher Voc and Jsc.

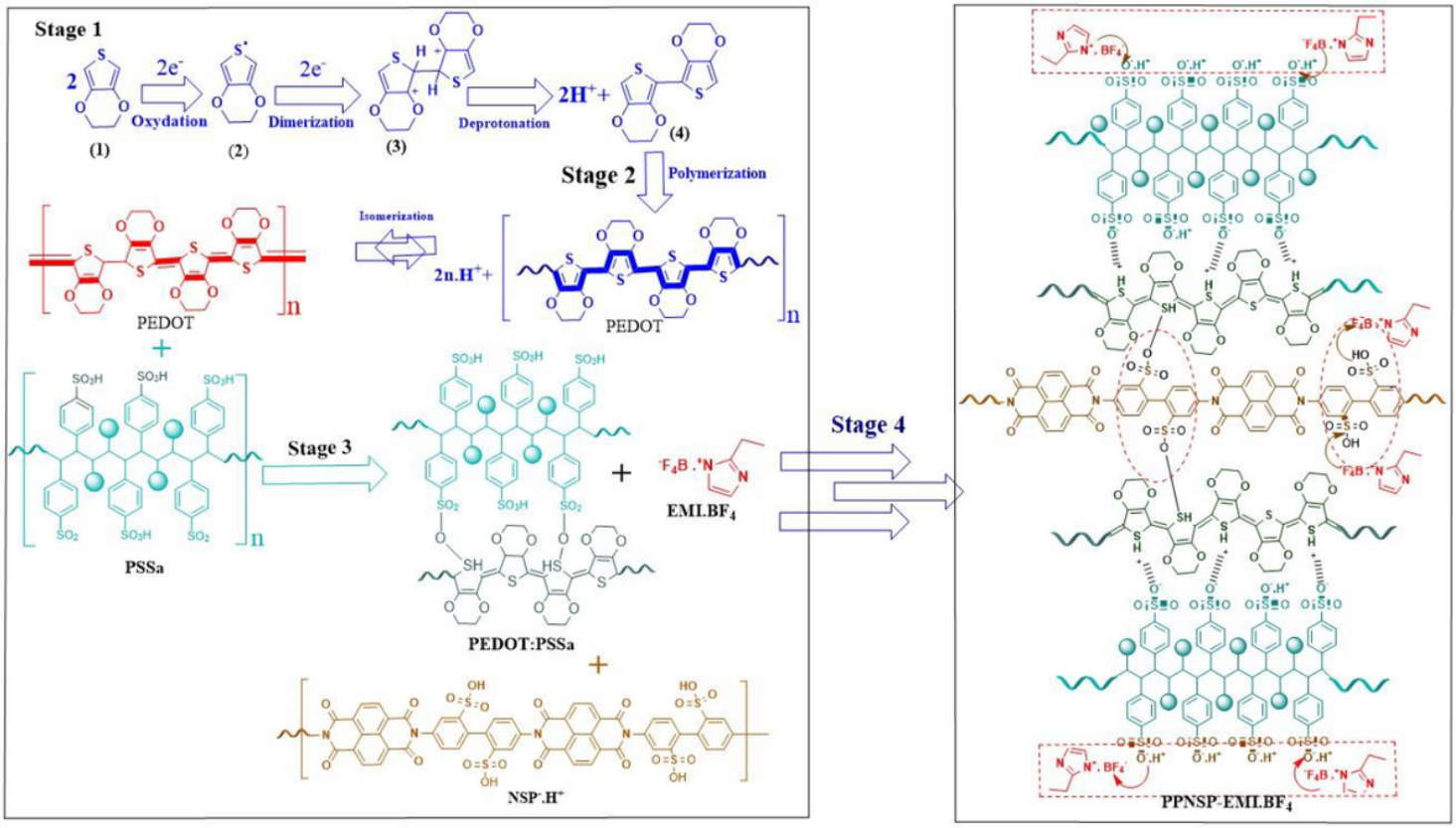

Figure 3

Mechanistic approach of the formation of oxidative and dimerization of EDOT, stage 1; polymerization and isomerization of EDOT, stage 2; Ionic interactions of EMI. BF4 with NSP-. H+, and PEDOT:PSSa, stage-3; and ion hopping mechanism between PPNSP and EMI. BF4, stage 4.

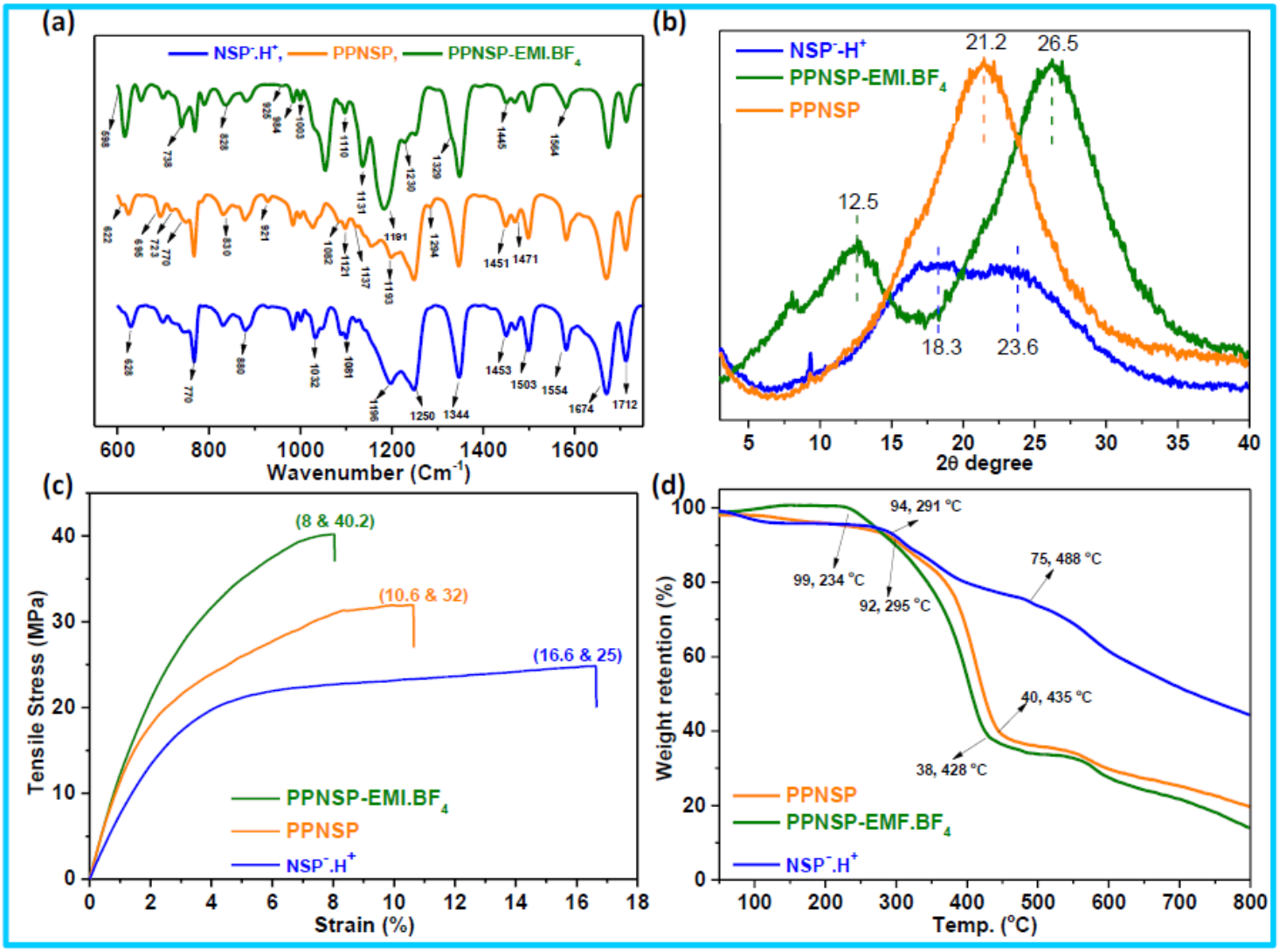

Figure 4

FT-IR (a); XRD (b); SS curves (c); and TGA curves (d) of NSP-.-H+, PPNSP, and PPNSP-EMI. BF4 composite e-skins

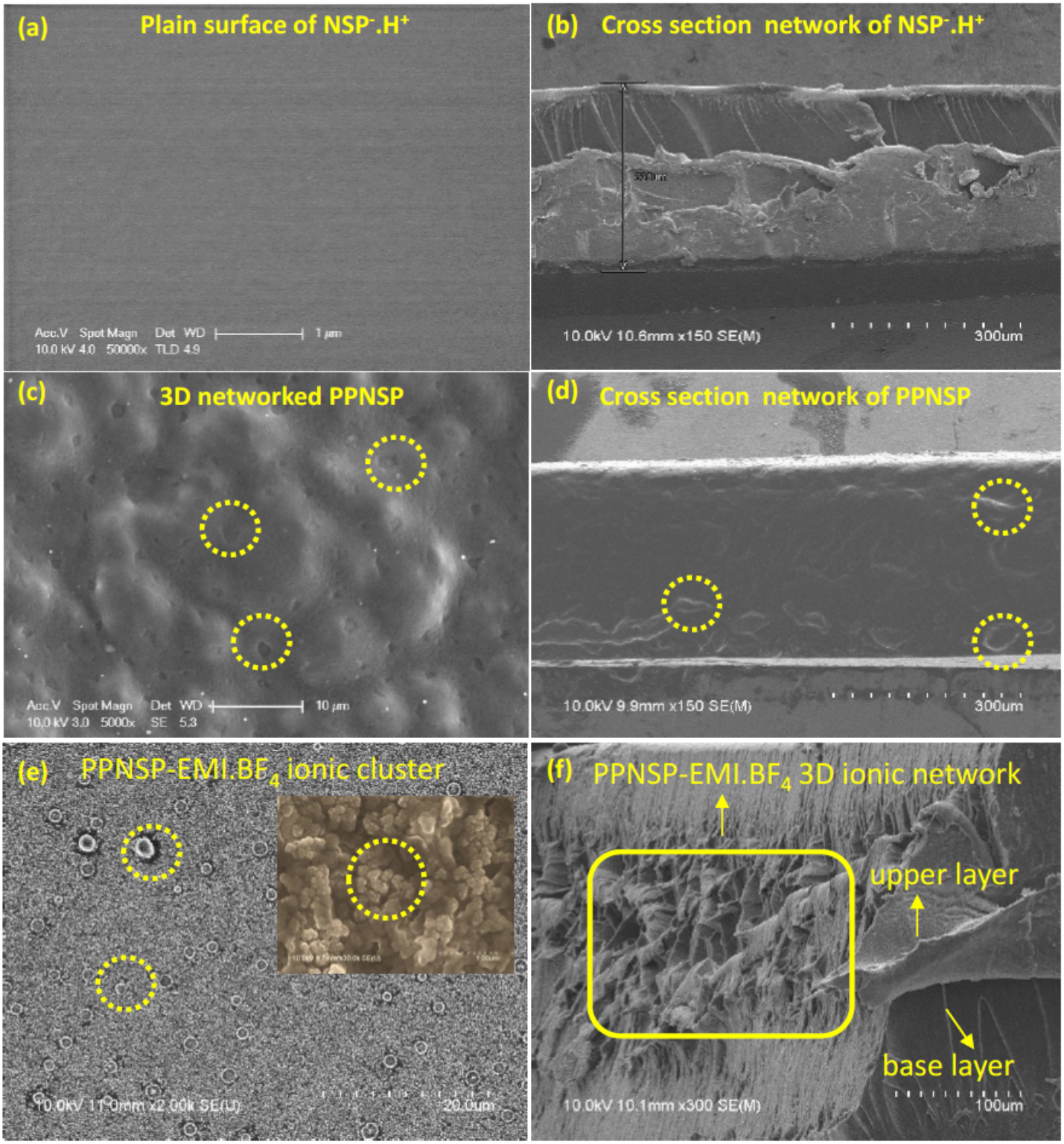

Figure 5

FE-SEM images of the surface morphologies of NSP. H+, PPNSP, and PPNSP-EMI. BF4 composite films; (a and b) regular plain surface; 3D networked submicron to micron hallow grooves and knots on the surface, (c, and d); ionic clusters on the surface of PPNSP film by aggregations of EMI. BF4, (inset image, strongly glued PPNSP-EMI. BF4 3D ionic clusters, which can help to promote the ion hopping mechanism, at 1 μm

magnification) (e), and loosely bonded 3D ionic networks in the cross-sectional view of PPNSP-EMI. BF4 composite film (f).

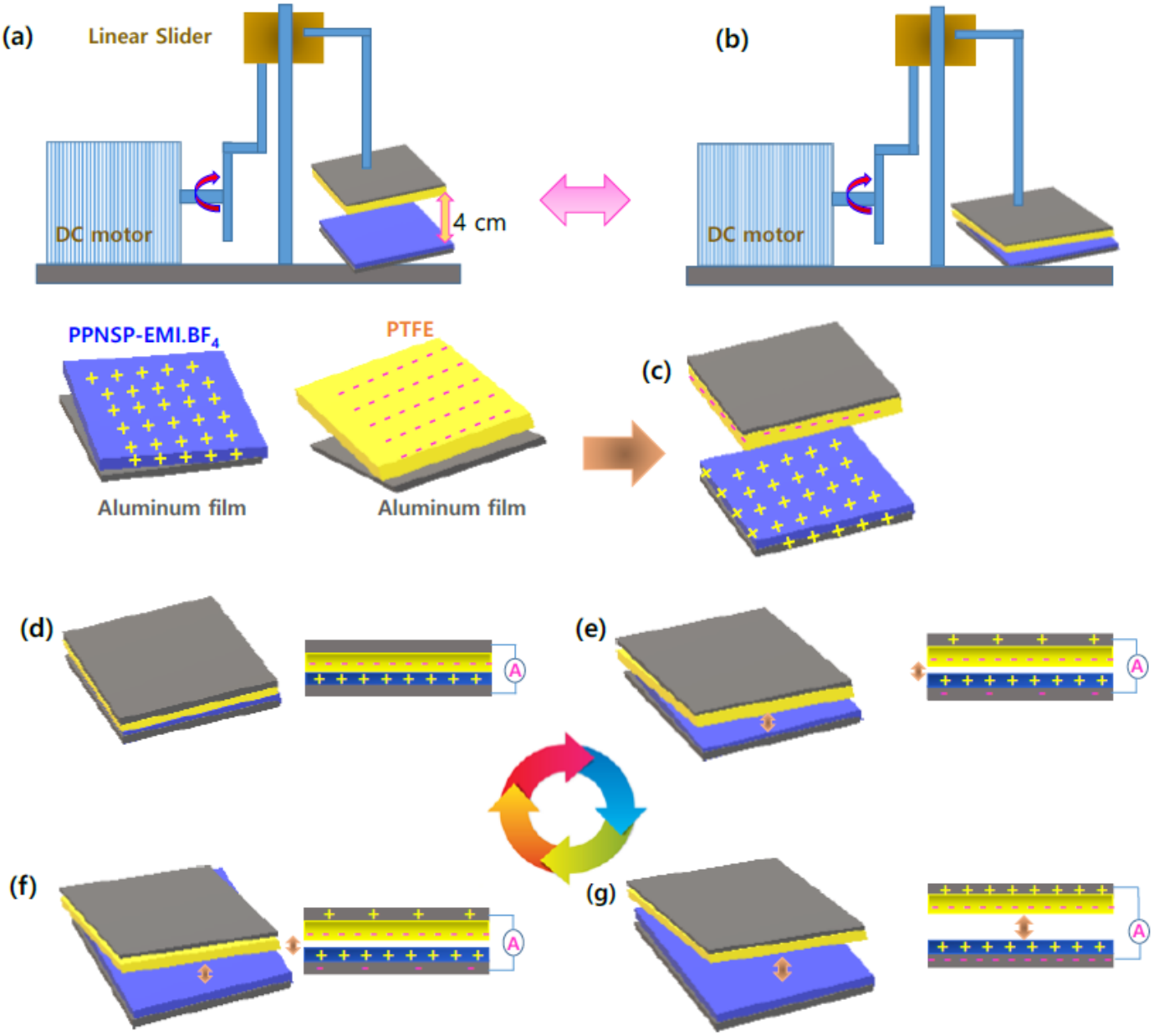

Figure 6

Mechanical operation of PPNSP-EMI.BF4 e-skin TENG at (a) separation state, (b) fully contacted state(c) initial condition, (d) full contacted, (e) separated, (f) fully separated condition and (g) contacted again of TENG results of NSP.H+, PPNSP, and PPNSP-EMI.BF4 e-Skin.

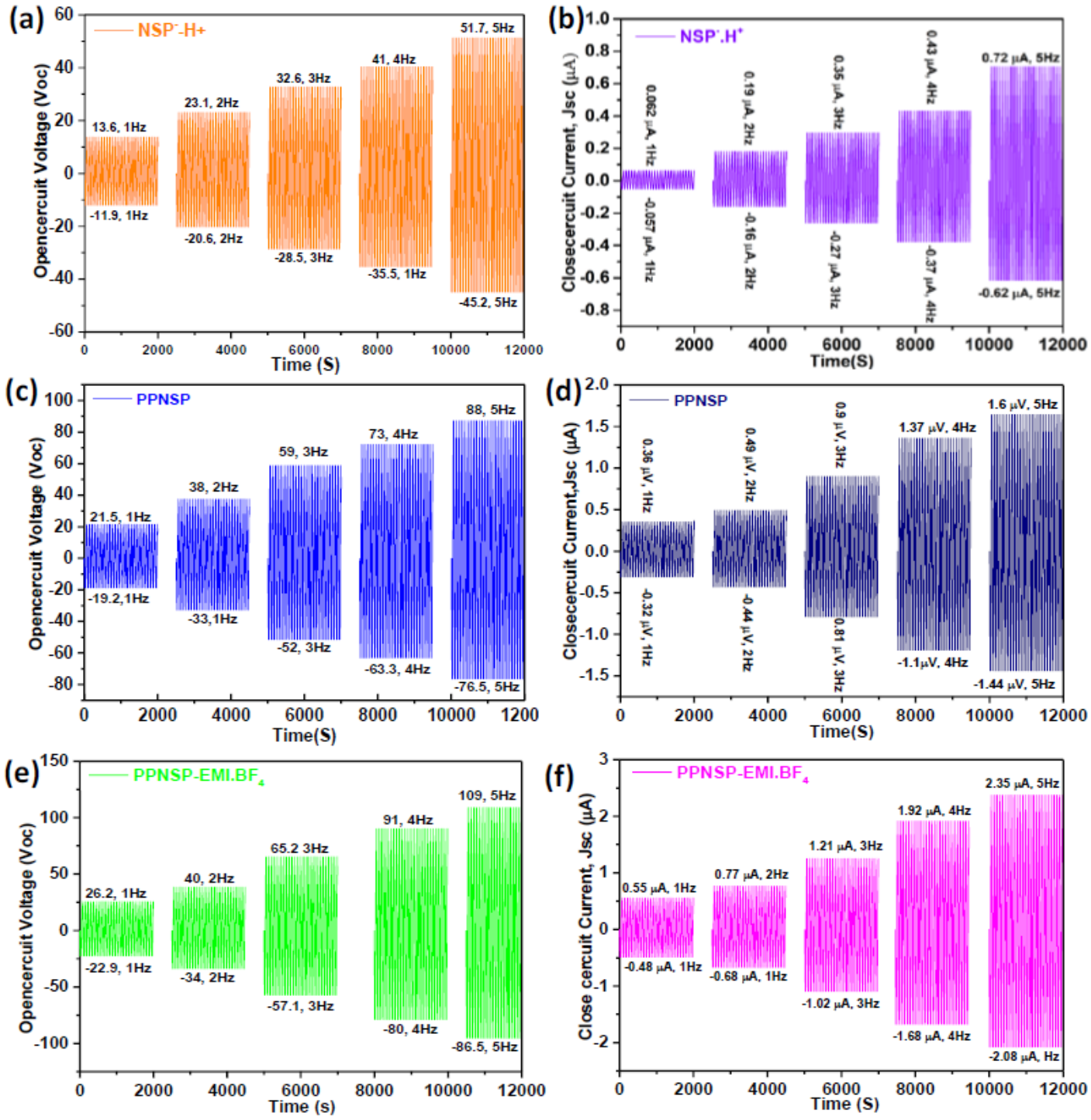

Figure 7

The output voltages (Voc) and close circuit currents (Jsc) under numerous feedback conditions in open circuit structures. The Voc and Isc of (a, b) NSP. H+-TENG; (c, d) PPNSP-TENG; and (e, f) PPNSP-EMI.BF4 e-skin-TENG.

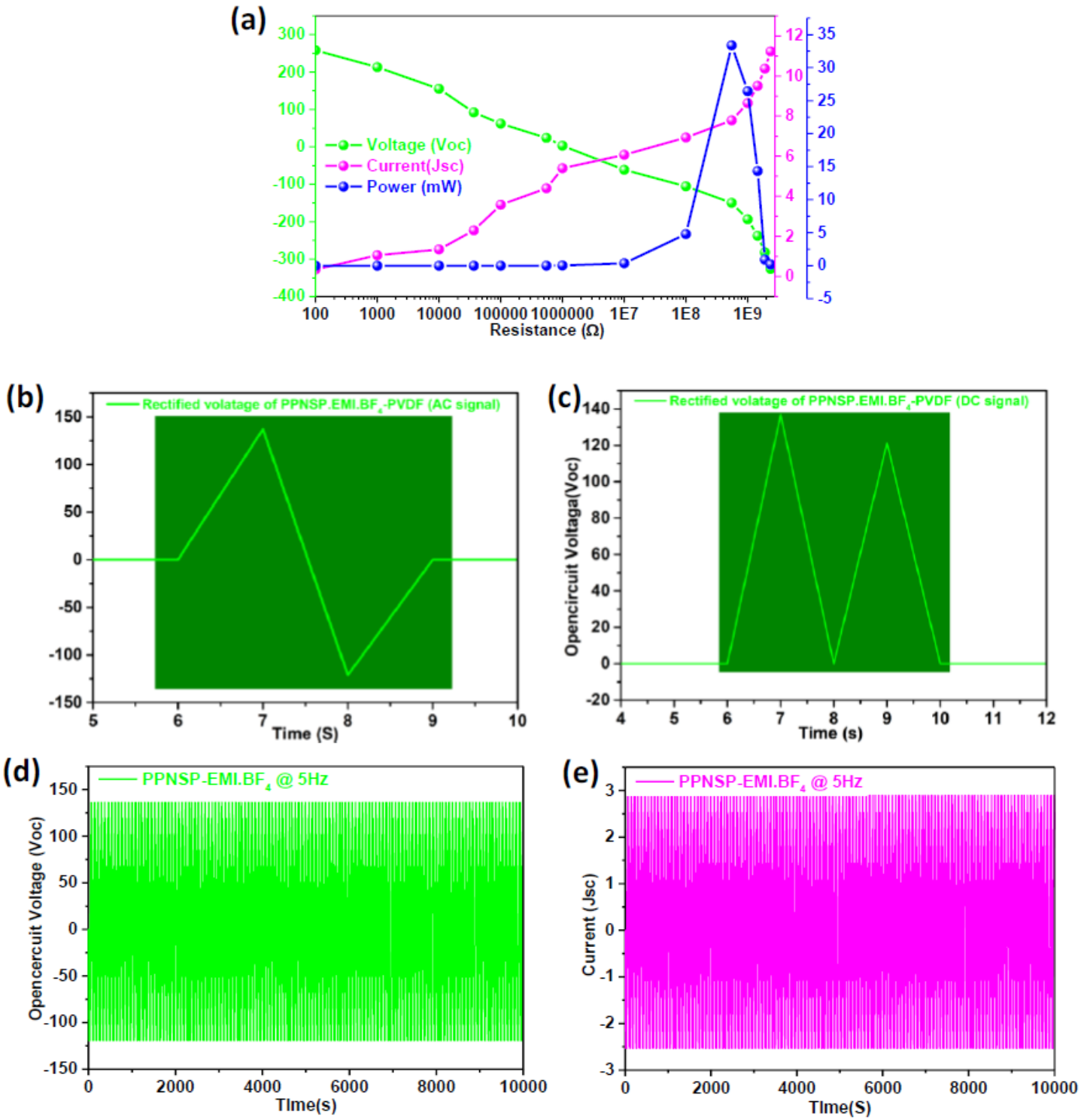

Figure 8

(a) Load resistance analysis and power density calculations of PPNSP.EMI.BF4-TENG such as open circuit voltage (Voc), short circuits current (Jsc), and power output, (mW) against external load resistances (Ω) at 5 Hz; (b) rectified voltage of AC signal, (c) DC signal; (d, and e), stability and durability performance tests of Voc and Jsc for 10000 cycles at 5 Hz.

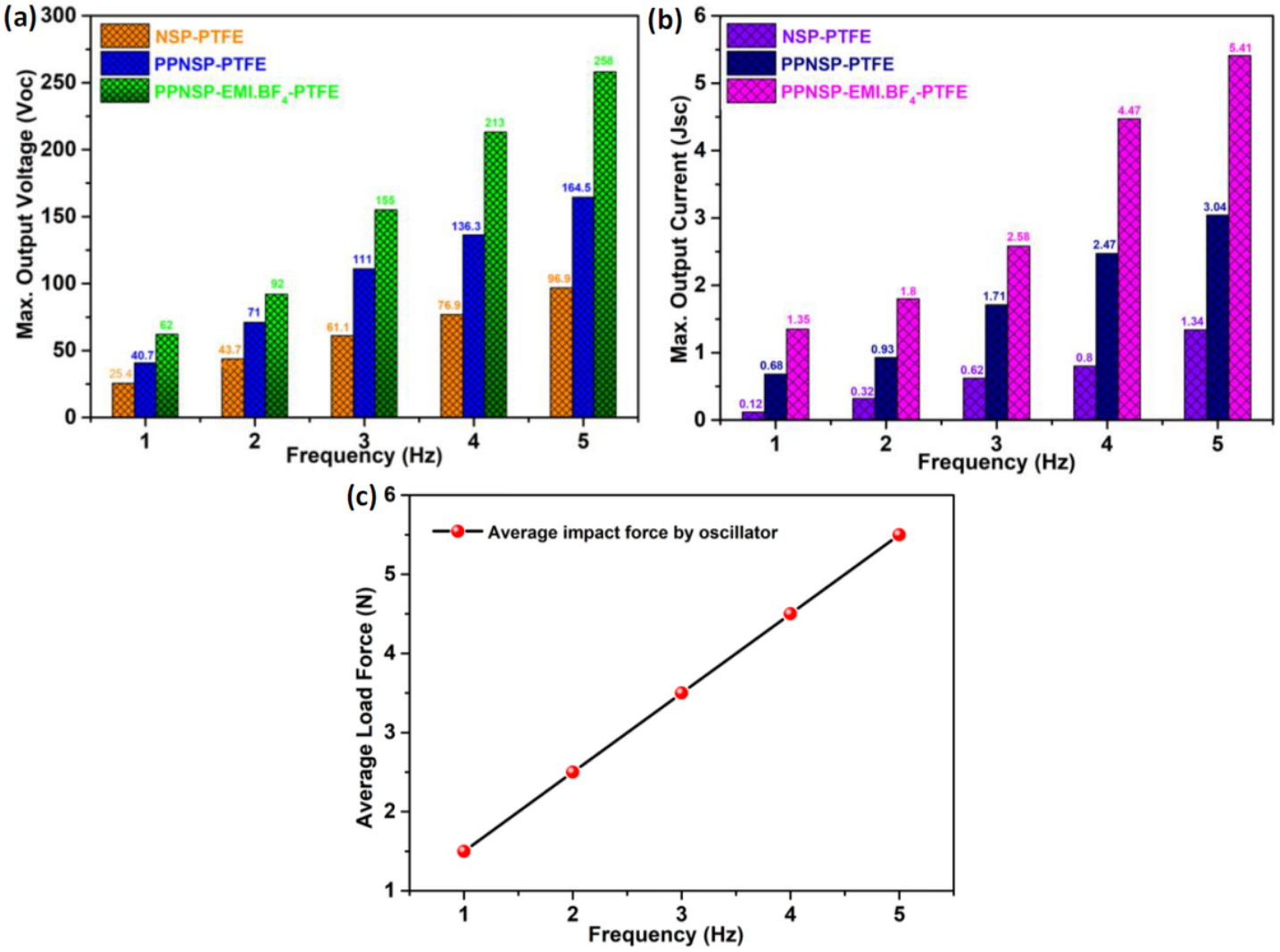

Figure 9

(a) The open circuit voltages (Voc); (b) short circuit currents of PPNSP.EMI.BF4 e-skin TENG at various applied frequencies; (c) Impact force at various applied frequencies.

Supplementary Files

This is a list of supplementary files associated with this preprint. Click to download.

- SupportingInformation.docx